The Astrophysical Journal, 633:11–22, 2005 November 1

TOPOLOGY ANALYSIS OF THE SLOAN DIGITAL SKY SURVEY. I. SCALE AND LUMINOSITY DEPENDENCE

Changbom Park,[1] Yun-Young Choi,[1] Michael S. Vogeley,[2] J. Richard Gott III,[3] Juhan Kim,[1]
Chiaki Hikage,[4] Takahiko Matsubara,[4] Myeong-Gu Park,[5] Yasushi Suto,[6] and David H. Weinberg[7]
(for the SDSS Collaboration)

Received 2005 March 25; accepted 2005 June 28

ABSTRACT

We measure the topology of volume-limited galaxy samples selected from a parent sample of 314,050 galaxies in the Sloan Digital Sky Survey (SDSS), which is now complete enough to describe the fully three-dimensional topology and its dependence on galaxy properties. We compare the observed genus statistic $G(\nu_f)$ to predictions for a Gaussian random field and to the genus measured for mock surveys constructed from new large-volume simulations of the ΛCDM cosmology. In this analysis we carefully examine the dependence of the observed genus statistic on the Gaussian smoothing scale R_G from 3.5 to 11 h^{-1} Mpc and on the luminosity of galaxies over the range $-22.50 < M_r < -18.5$. The void multiplicity A_V is less than unity at all smoothing scales. Because A_V cannot become less than 1 through gravitational evolution, this result provides strong evidence for biased galaxy formation in low-density environments. We also find clear evidence of luminosity bias of topology within the volume-limited subsamples. The shift parameter $\Delta\nu$ indicates that the genus of brighter galaxies shows a negative shift toward a "meatball" (i.e., cluster dominated) topology, while faint galaxies show a positive shift toward a "bubble" (i.e., void dominated) topology. The transition from negative to positive shift occurs approximately at the characteristic absolute magnitude $M_{r*} = -20.4$. Even in this analysis of the largest galaxy sample to date, we detect the influence of individual large-scale structures, as the shift parameter $\Delta\nu$ and cluster multiplicity A_C reflect (at $\sim 3\,\sigma$) the presence of the Sloan Great Wall and an X-shaped structure that runs for several hundred megaparsecs across the survey volume.

Subject heading: large-scale structure of universe

Online material: color figures

1. INTRODUCTION

Topology analysis was introduced in cosmology as a method to test the Gaussianity of the primordial density field as predicted by many inflationary scenarios (Gott et al. 1986). The statistics of the initial density field are thought to be well preserved at large scales, where structures are still in the linear regime. Therefore, to achieve the original purpose of topology analysis, one needs to use large observational samples and explore the galaxy density field at large smoothing scales. This requires an accurate map of the large-scale distribution of galaxies over scales of several hundred megaparsecs, as is now available from the Sloan Digital Sky Survey (SDSS).

On smaller scales in the nonlinear regime, the topology of the galaxy distribution yields strong constraints on the galaxy formation mechanisms and the background cosmogony. Galaxies of various species are distributed in different ways in space, and the differences can be quantitatively measured by topology analysis. By studying galaxy biasing as revealed in statistics beyond the two-point correlation function and power spectrum, the complex nature of galaxy formation can be better understood. The topology statistics can be precision measures of the galaxy formation process (Park et al. 2005). To examine topology at small scales it is necessary to use dense galaxy redshift samples that are also large enough in volume not to be significantly affected by sample variance. Using the SDSS, it is now possible to study the topology of the galaxy distribution down to a Gaussian smoothing scale of 3 h^{-1} Mpc in volume-limited samples that include galaxies as faint as absolute magnitude $M_r = -18$ while still maintaining reasonably large sample volumes.

Previous topological analyses of SDSS galaxy distribution include the two-dimensional genus (Hoyle et al. 2002), three-dimensional genus with the Early Data Release (Hikage et al. 2002), and Minkowski functionals with sample 12 (Hikage et al. 2003). The present paper updates the previous results with the latest SDSS sample, described below as sample 14. For the first time, we are able to detect the quantitative signature of luminosity-dependent biasing by characterizing the genus curves in terms of the statistical quantities $\Delta\nu$, A_V, and A_C: $\Delta\nu$ is the shift parameter, and A_V and A_C are cluster and void abundance parameters, respectively.

In this paper we adopt the genus statistic as a measure of the topology of the smoothed galaxy number density field. To study the impact of galaxy biasing, we limit our attention to small-scale topology, over a range of Gaussian smoothing scales from 3.5 to 11 h^{-1} Mpc. We examine the scale dependence of topology to see if there are differences with respect to the ΛCDM model. We also detect the luminosity bias in the topology of large-scale structure. In § 2 we briefly describe the SDSS and define our volume-limited

[1] Korea Institute for Advanced Study, Dongdaemun-gu, Seoul 130-722, South Korea.
[2] Department of Physics, Drexel University, 3141 Chestnut Street, Philadelphia, PA 19104.
[3] Department of Astrophysical Sciences, Princeton University, Peyton Hall, Princeton, NJ 08544-1001.
[4] Department of Physics and Astrophysics, Nagoya University, Chikusa, Nagoya 464-8603, Japan.
[5] Department of Astronomy and Atmospheric Sciences, Kyungpook National University, Daegu 702-701, South Korea.
[6] Department of Physics, School of Science, University of Tokyo, Tokyo 113-0033, Japan.
[7] Department of Astronomy, Ohio State University, 140 West 18th Avenue, Columbus, OH 43210.

SDSS samples. In § 3 we define the topology statistics and describe our genus analysis procedure. Section 4 describes our new *N*-body simulation, which we use for constructing mock surveys and testing for systematic effects. In § 5 we present results of tests for scale and luminosity dependences of the observed genus curves. We discuss our findings in § 6.

2. OBSERVATIONAL DATA SET

2.1. *Sloan Digital Sky Survey*

The SDSS (York et al. 2000; Stoughton et al. 2002; Abazajian et al. 2003, 2004) is a survey to explore the large-scale distribution of galaxies and quasars and their physical properties using a dedicated 2.5 m telescope at Apache Point Observatory. The photometric survey has been nearly completed, covering about 2.8 sr of the northern Galactic cap in five photometric bandpasses denoted by *u*, *g*, *r*, *i*, and *z* centered at 3551, 4686, 6165, 7481, and 8931 Å, respectively, by an imaging camera with 54 CCDs (Fukugita et al. 1996; Gunn et al. 1998). The limiting magnitudes of photometry at a signal-to-noise ratio of 5:1 are 22.0, 22.2, 22.2, 21.3, and 20.5 in the five bandpasses, respectively. The width of the point-spread function is 1.″4, and the photometric uncertainties are 2% rms (Abazajian et al. 2004). Roughly 5×10^7 galaxies will be cataloged.

After image processing (Lupton et al. 2001; Stoughton et al. 2002; Pier et al. 2003) and calibration (Hogg et al. 2001; Smith et al. 2002), targets are selected for spectroscopic follow-up observation. The spectroscopic survey is planned to continue through 2008 as the Legacy survey and to produce about 10^6 galaxy spectra. The spectra are obtained by two dual fiber-fed CCD spectrographs. The spectral resolution is $\lambda/\Delta\lambda \sim 1800$, and the rms uncertainty in the redshift is $\sim$30 km s^{-1}. Mainly due to the minimum distance of 55″ between fibers, incompleteness of the spectroscopic survey reaches about 6% (Blanton et al. 2003a) in such a way that regions with high surface densities of galaxies become less prominent. This angular variation of the sampling density is accounted for in our analysis.

The SDSS spectroscopy yields three major samples: the main galaxy sample (Strauss et al. 2002), the luminous red galaxy sample (Eisenstein et al. 2001), and the quasar sample (Richards et al. 2002). The main galaxy sample is a magnitude-limited sample with an apparent Petrosian *r*-magnitude cut of $m_{r,\rm lim} \approx 17.77$, which is the limiting magnitude for spectroscopy (Strauss et al. 2002). It has a further cut in Petrosian half-light surface brightness $\mu_{R50,\rm limit} = 24.5$ mag arcsec^{-2}.[8]

In our topology analysis, we use a large-scale structure sample of the SDSS from the New York University Value-Added Galaxy Catalog (NYU-VAGC; Blanton et al. 2005). As of the writing of this paper, the most up-to-date large-scale structure sample is sample 14, which covers 3836 deg^2 of the sky and contains 314,050 galaxies with redshifts between 0.001 and 0.5, surveyed as of 2003 November. The large-scale structure sample also comes with an angular selection function of the survey defined in terms of spherical polygons (Hamilton & Tegmark 2004), which takes into account the incompleteness due to mechanical spectrograph constraints, bad spectra, or bright foreground stars.

2.2. *Sample Definitions for Genus Analysis*

To study the three-dimensional topology of the smoothed galaxy number density distribution, it is advantageous for the observational sample to have the lowest possible surface-to-volume ratio. For this reason we trim sample 14 as shown in Figure 1, where the solid gray lines delineate our sample boundaries in the survey coordinate plane (λ, η). We discard the three southern stripes and the small areas protruding or isolated from the main surveyed regions. These cuts decrease the number of galaxies from 314,050 to 239,216 in two analysis regions. Within our sample boundaries, we account for angular variation of the survey completeness by using the angular selection function provided with the large-scale structure sample data set. To facilitate our analysis, we make two arrays of square pixels of size $0.^\circ025 \times 0.^\circ025$ in the (λ, η) sky coordinates, which cover the two analysis regions, and store the angular selection function calculated using the MANGLE routine (Hamilton & Tegmark 2004). At the location of each pixel, the routine calculates the survey completeness in a spherical polygon formed by the adaptive tiling algorithm (Blanton et al. 2003a) used for the SDSS spectroscopy. The resulting useful area within the analysis regions with nonzero selection function is 0.89 sr.

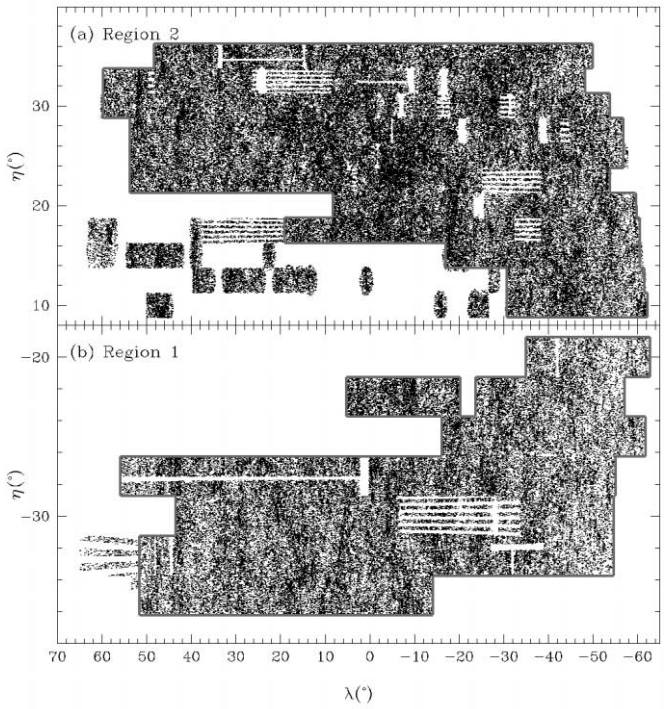

FIG. 1.—Angular definition of the SDSS sample used for our topology analysis. Solid gray lines delineate the boundaries of the analysis regions in the survey coordinate plane (λ, η). [*See the electronic edition of the Journal for a color version of this figure*.]

Analysis region 1 contains the famous "Sloan Great Wall," for which redshift slices are shown by Gott et al. (2005). Figure 2 shows galaxies with $14.5 \leq m_r \leq 17.5$ in two $7.^\circ5$ thick slices in analysis region 2. We assume a flat ΛCDM cosmology with $\Omega_m = 0.3$ to convert redshifts to comoving coordinates. In the top slice of Figure 2 there is a weak wall of galaxies that extends over $\sim$700 h^{-1} Mpc at comoving distance of roughly $r =$ 400 h^{-1} Mpc. Void, wall, and filamentary structures of galaxies are seen through these slices. A roughly spherical void of size $\sim$100 h^{-1} Mpc in diameter is seen in the slices at distance of about 200 h^{-1} Mpc. In the bottom slice there is a $\sim$300 h^{-1} Mpc–sized structure that looks like a runner or an X, formed by several neighboring voids of various sizes, as was the structure in the CfA slice (Geller & Huchra 1989). We note several small voids nested within larger ones.

[8] More details about the survey can be found at http://www.sdss.org/dr3/.

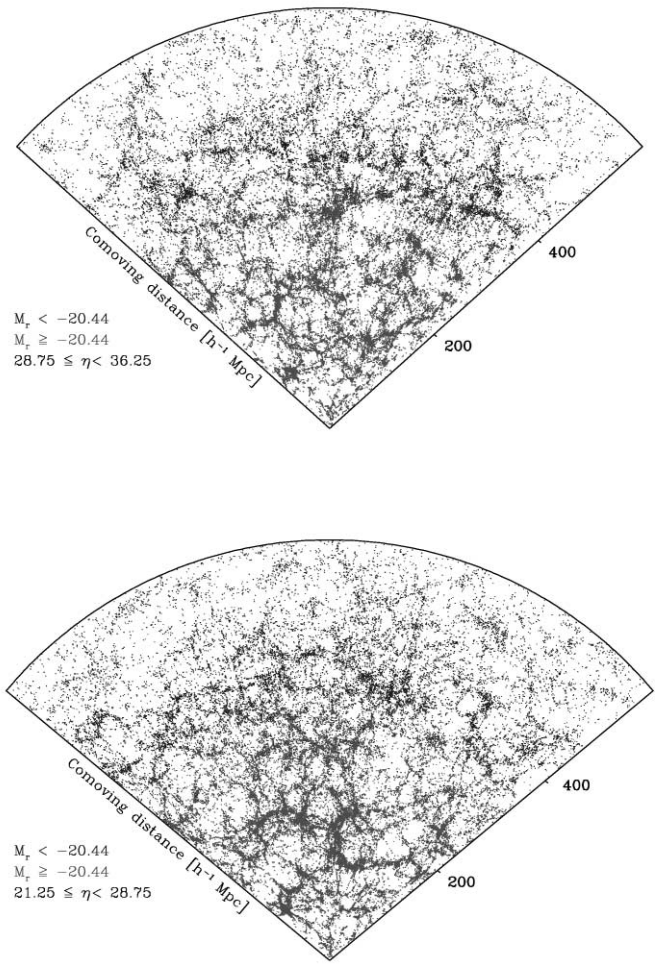

FIG. 2.—Distribution of galaxies with $14.5 \leq m_r \leq 17.5$ in two contiguous 7.°5 thick slices in analysis region 2. The radial coordinate is the comoving distance, and the angular coordinate is the SDSS survey longitude λ. [*See the electronic edition of the Journal for a color version of this figure*.]

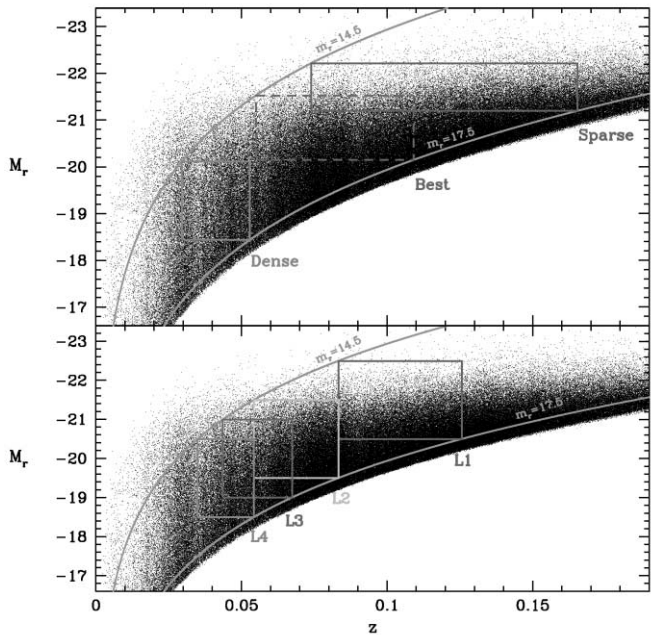

FIG. 3.—Sample definitions in redshift–absolute magnitude space. The top panel shows boundaries of three volume-limited samples used for studying the scale dependence of topology. In the bottom panel, four samples used for luminosity bias study are defined. The smooth curves delineate the sample boundaries corresponding to our choice of apparent magnitude limits of $14.5 \leq m_r \leq 17.5$. [*See the electronic edition of the Journal for a color version of this figure*.]

In our topology analysis we use only volume-limited samples of galaxies defined by absolute magnitude limits. Figure 3 shows galaxies in sample 14 in redshift–absolute magnitude space. The smooth curves delineate the sample boundaries corresponding to our choice of apparent magnitude limits of $14.5 \leq m_r \leq 17.5$, after correction for Galactic reddening (Schlegel et al. 1998). The faint limit of $m_r = 17.5$ is slightly brighter than the spectroscopic selection criterion of $m_r < 17.77$ to allow use of some early data that used a brighter limit. The bright-end apparent magnitude limit of $m_r = 14.5$ is imposed to avoid small incompleteness that is caused by the exclusion of galaxies with large central surface brightness (to avoid spillover in the spectrograph CCDs) and associated with the quality of deblending of large galaxies. The most natural volume-limited sample is that containing the maximum number of galaxies. We vary the faint and bright absolute magnitude limits to find such a sample and label this our "best" sample. It is defined by absolute magnitude limits $-21.53 \leq M_r < -20.15$, which correspond to a comoving distance range of $162.9 < r < 319.0\ h^{-1}$ Mpc or a redshift range of $0.055 < z < 0.109$ when the apparent magnitude cut is applied. The comoving distance and redshift limits are obtained using the formula

$$m_r - M_r = 5 \log [r(1+z)] + 25 + K(z), \qquad (1)$$

where $K(z)$ is the K-correction and $r(1+z)$ is the luminosity distance. We use a polynomial fit to the mean K-correction within $0 < z < 0.3$,

$$K(z) = 2.3537(z-0.1)^2 + 1.04423(z-0.1) - 2.5\log(1+0.1). \qquad (2)$$

The rest-frame absolute magnitudes of galaxies in sample 14 are computed in fixed bandpasses, shifted to $z = 0.1$, using Galactic reddening corrections and K-corrections (for a full description, see Hogg et al. [2002] and Blanton et al. [2003b]). This means that galaxies at $z = 0.1$ have a K-correction of $-2.5 \log (1 + 0.1)$, independent of their spectral energy distributions. We do not take into account galaxy evolution effects. The definition of the best sample is shown in Figure 3 and Table 1.

The top panel of Figure 3 also shows the absolute magnitude and redshift limits for two additional samples, which we label "sparse" and "dense" because of their mean densities relative to the best sample. The dense sample has a bright absolute magnitude limit just below the faint limit of the best sample. The faint limit of the dense sample is determined by maximizing the number of galaxies. For the sparse sample, the bright absolute magnitude limit was chosen to be fainter than -22.22, above which galaxies in sample 14 are missing at far distances. The faint limit of the sparse sample is determined by maximizing the number of galaxies contained in the sample. In what follows, these samples are used to study the dependence of topology on scale.

The bottom panel of Figure 3 shows the absolute magnitude and redshift limits of four samples that we use to study the luminosity dependence of topology. Each sample has an absolute magnitude range of two magnitudes. The brightest sample, L1, has a bright magnitude limit of $M_r = -22.5$. Each luminosity sample is further divided into three subsamples as defined in

TABLE 1
VOLUME-LIMITED LUMINOSITY AND SCALE DEPENDENCE SAMPLES

Sample Name	Absolute Magnitude	Redshift	Distance[a]	No. of Galaxies	N_{res}[b]
		Scale Dependence			
Sparse	$-22.22 \leq M_r < -21.20$	$0.0740 < z < 0.1654$	$218.2 < r < 477.1$	20138	3618
Best	$-21.53 \leq M_r < -20.15$	$0.0550 < z < 0.1091$	$162.9 < r < 319.0$	36000	6466
Dense	$-20.12 \leq M_r < -18.44$	$0.0295 < z < 0.0529$	$88.0 < r < 156.8$	13011	2336
		Luminosity Dependence			
L1	$-22.50 \leq M_r < -20.50$	$0.0833 < z < 0.1257$	$245.1 < r < 366.1$	27623	4961
L1-1	$-22.50 \leq M_r < -20.87$	...	...	13811	2481
L1-2	$-21.16 \leq M_r < -20.66$	...	...	13811	2481
L1-3	$-20.87 \leq M_r < -20.50$	...	...	13811	2481
L2	$-21.50 \leq M_r < -19.50$	$0.0543 < z < 0.0833$	$160.9 < r < 245.1$	29932	5374
L2-1	$-21.50 \leq M_r < -20.09$	...	...	14966	2687
L2-2	$-20.52 \leq M_r < -19.77$	...	...	14966	2687
L2-3	$-20.09 \leq M_r < -19.50$	...	...	14966	2687
L3	$-21.00 \leq M_r < -19.00$	$0.0436 < z < 0.0674$	$129.6 < r < 198.9$	19315	3468
L3-1	$-21.00 \leq M_r < -19.70$	...	...	9657	1734
L3-2	$-20.17 \leq M_r < -19.32$	...	...	9657	1734
L3-3	$-19.70 \leq M_r < -19.00$	...	...	9657	1734
L4	$-20.50 \leq M_r < -18.50$	$0.0350 < z < 0.0543$	$104.1 < r < 160.9$	13107	2353
L4-1	$-20.50 \leq M_r < -19.29$	...	...	6553	1177
L4-2	$-19.76 \leq M_r < -18.87$	...	...	6553	1177
L4-3	$-19.29 \leq M_r < -18.50$	...	...	6553	1177

NOTE.—The samples are volume limited with apparent magnitude limits of $14.5 \leq m_r \leq 17.5$.
[a] Comoving distance in units of h^{-1} Mpc.
[b] Number of resolution elements calculated by $\Omega(r_{max}^3 - r_{min}^3)/3(2\pi)^{3/2}\bar{d}^3$, where Ω is the solid angle of our analysis area and $\bar{d}$ is the mean separation of galaxies listed in Table 2.

Table 1. Each subsample has half the number of galaxies contained in its parent sample, and the brightest subsample does not overlap with the faintest one in absolute magnitude. Because the subsamples occupy the same volume of the universe and contain the same number of galaxies, differences among them are free from sample variance and Poisson fluctuation; any variation in topology is purely due to difference in the absolute magnitude of the galaxies.

3. THEORY FOR TOPOLOGY ANALYSIS

3.1. *Genus and Its Related Statistics*

The genus is a measure of the topology of isodensity contour surfaces in a smoothed galaxy density field. It is defined as

$$G = \text{Number of holes in contour surfaces} - \text{Number of isolated regions} \quad (3)$$

in the isodensity surfaces at a given threshold level. The Gauss-Bonnet theorem connects the global topology with an integral of local curvature of the surface S, i.e.,

$$G = -\frac{1}{4\pi}\int_S \kappa\, da, \quad (4)$$

where κ is the local Gaussian curvature. In the case of a Gaussian field, the genus per volume as a function of density threshold level is known (Doroshkevich 1970; Adler 1981; Hamilton et al. 1986),

$$g(\nu) = g(0)\left(1-\nu^2\right)e^{-\nu^2/2}, \quad (5)$$

where $\nu \equiv (\rho - \bar{\rho})/\sigma$ is the threshold density in units of standard deviations $\sigma = \langle(\rho-\bar{\rho})^2\rangle^{1/2}$ from the mean. The amplitude is

$$g(0) = \frac{1}{(2\pi)^2}\left(\frac{\langle k^2\rangle}{3}\right)^{3/2},$$

where

$$\langle k^2\rangle = \frac{\int P(k)k^2\, d^3k}{\int P(k)\, d^3k}$$

depends on the power spectrum $P(k)$ of the smoothed density field. To separate variation in topology from change of the one-point density distribution, we measure the genus as a function of the volume-fraction threshold ν_f. This parameter defines the density contour surface such that the volume fraction in the high-density region is the same as the volume fraction in a Gaussian random field contour surface with a value of $\nu = \nu_f$. Any deviation of the observed genus curve from the Gaussian one is evidence for non-Gaussianity of the primordial density field and/or that acquired due to the nonlinear gravitational evolution or galaxy biasing. There have been a number of studies on the effects of non-Gaussianity on the genus curve (Weinberg et al. 1987; Park & Gott 1991; Park et al. 2005).

To measure the deviation of the genus curve from Gaussian, several statistics have been suggested. First is the amplitude drop, $R = G_{obs}/G_G$, where G_{obs} is the amplitude of the observed genus curve and G_G is that of a Gaussian field that has the observed power spectrum (Vogeley et al. 1994). It is a measure of the phase correlation produced by the initial non-Gaussianity, the gravitational evolution, and the galaxy biasing. We do not calculate R in this paper and defer it to later works in which we will

examine the genus over a larger range of smoothing scales that include the linear regime. Here we simply measure the observed genus amplitude $G_{\rm obs}$ to test for scale and luminosity dependence. We measure $G_{\rm obs}$ by finding the best-fitting Gaussian genus curve over $-1 \leq \nu \leq 1$.

The shift parameter $\Delta\nu$ is defined as

$$\Delta\nu = \frac{\int d\nu\, G_{\rm obs}(\nu)\nu}{\int d\nu\, G_{\rm fit}(\nu)}, \tag{6}$$

where the integral is over $-1 \leq \nu \leq 1$ and $G_{\rm obs}$ and $G_{\rm fit}$ are the observed and the best-fit Gaussian genus curves, respectively (Park et al. 1992). It measures the threshold level at which topology is maximally spongelike. For a density field dominated by voids, $\Delta\nu$ is positive and we say that the density field has a "bubble-like" topology. For a cluster-dominated field, $\Delta\nu$ is negative and we say that the field has a "meatball-like" topology.

The abundances of clusters and voids relative to that expected for a Gaussian random field are measured by the parameters A_C and A_V. These parameters are defined by

$$A = \frac{\int d\nu\, G_{\rm obs}(\nu)}{\int d\nu\, G_{\rm fit}(\nu)}, \tag{7}$$

where the integration intervals are $+1.2 < \nu_f < +2.2$ for A_C and $-2.2 < \nu_f < -1.2$ for A_V (Park et al. 2001, 2005). These intervals are centered near the minima of the Gaussian genus curve ($\nu = \pm\sqrt{3}$) and stay away from the thresholds at which the genus curve is often affected by the shift phenomenon. These ranges also exclude extreme thresholds at which for low-density regions the volume-fraction threshold level ν_f is very sensitive to the density value. These parameters are defined so that $A_{C,V} > 1$ means that more independent clusters or voids are observed than are predicted by a Gaussian field at a fixed volume fraction, whereas $A_{C,V} > 1$ means that fewer independent clusters or voids are seen. A detailed study of the effects of the gravitational evolution, the galaxy biasing, and the cosmogony on the $\Delta\nu$, A_V, and A_C statistics is presented by Park et al. (2005).

3.2. *Analysis Procedure*

To measure the genus using the CONTOUR3D algorithm (Weinberg 1988), we prepare an estimate of the smoothed density field on a grid, with pixels that lie outside the survey region flagged. Figure 1 together with the angular selection function table defines our angular mask. Table 1 lists the distance range for each sample. Using the angular mask and distance limits, we make a three-dimensional mask array of size 512^3 for each sample. The pixel size is always restricted to be slightly smaller than $R_{\rm G}/3$, where $R_{\rm G}$ is the Gaussian smoothing length. The Earth is located at the center of one face of the cubic array that forms the *x*-*z* plane. This mask array contains zeros in pixels that lie outside the boundaries shown in Figure 1. Mask array pixels that lie within the boundaries are assigned a selection function value read off from the angular selection function table. Because that table consists of fine pixels of $1'.5$ size, the mask array faithfully represents the survey selection effects. We also make a 512^3 galaxy density array into which we bin the SDSS galaxies that fall inside our sample boundaries. After a Gaussian smoothing length $R_{\rm G}$ is chosen, both the mask array and the galaxy density array are smoothed and divided by each other in the sense of $\rho_g/\rho_{\rm mask}$. This yields an array of smoothed galaxy density estimates that accounts for both the angular selection function and the effect of the survey boundary. In regions of the ratio array for which the corresponding value in the smoothed mask array value is smaller than 0.69, we flag the ratio array with negative values to indicate that they are outside the analysis region. This removes not only regions that are formally outside the survey volume, but also regions that are too close to the survey boundary, where the signal-to-noise ratio of the estimated density field is low. We choose a threshold value of 0.69 as a compromise between homogeneous smoothing and a larger survey volume. This value corresponds to the value of a smoothed mask at a distance of $0.5R_{\rm G}$ inside an infinite planar survey boundary. Figure 4 shows the mask array for the best sample after smoothing and trimming. Figure 5 shows the best sample smoothed in the way explained above. The left two figures of Figure 5 show underdense regions at volume fractions of 7% and 50%. The two right figures show overdense regions. The Sloan Great Wall is visible in region 1 at a 7% high-density level.

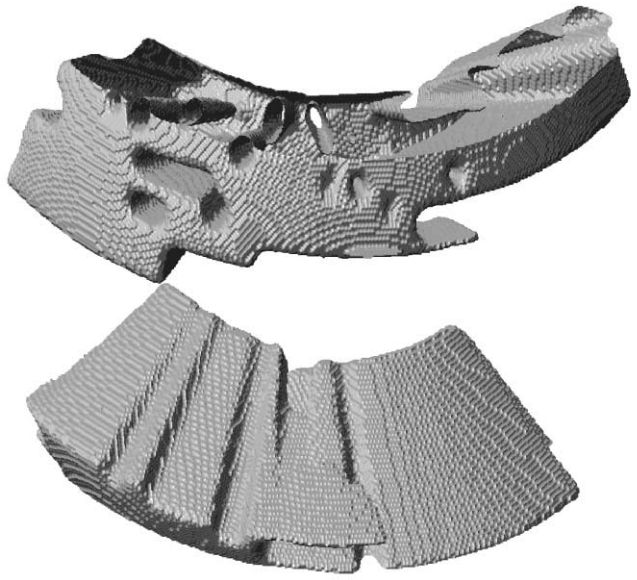

FIG. 4.—Three-dimensional views of the mask array looking toward the Earth from the far side after smoothing and trimming. This mask is used for analysis of the best sample. The top piece is region 2, and the bottom one is region 1.

After the smoothed galaxy density field is obtained, we compute the genus at each volume fraction ν_f using CONTOUR3D. We then estimate the best-fit Gaussian amplitude $G_{\rm obs}$ and the other genus-related parameters, $\Delta\nu$, A_V, and A_C, for each genus curve $G(\nu_f)$.

4. MOCK SURVEYS FROM SIMULATIONS

To measure the topology statistics accurately and to detect any weak non-Gaussianity or dependence of topology on the physical properties of galaxies, accurate modeling of the survey and the analysis are required to eliminate systematic effects. For this purpose we have made a new large *N*-body simulation of a ΛCDM universe, which has a mean particle number density that is much higher than that of the galaxies in the SDSS and at the same time can safely contain the large-scale modes that modulate the density field over the maximum scales explored by the SDSS. We adopt the cosmological parameters measured by the *Wilkinson Microwave Anisotropy Probe* (*WMAP*; Spergel et al. 2003), which are $\Omega_m = 0.27$, $\Omega_b = 0.0463$, $\Omega_\Lambda = 0.73$, $h = 0.71$, and $\sigma_8 = 0.9$. Here σ_8 is the rms fluctuation of mass in a 8 h^{-1} Mpc radius spherical top hat. The physical size of the simulation cube is 5632 h^{-1} Mpc, which is much larger than any volume-limited

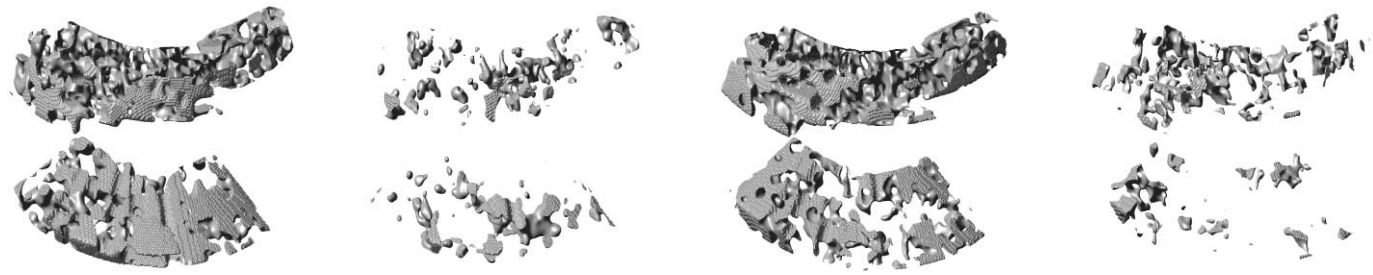

FIG. 5.—Three-dimensional view of the galaxy number density field of the best sample after smoothing and trimming. On the left, density contours enclose low-density regions occupying 7% and 50% of the volume, and on the right, contours enclose high-density regions filling 50% and 7% of the volume of the best sample.

SDSS sample we use here. The simulation follows the evolution of 8 billion =2048^3 cold dark matter (CDM) particles whose initial conditions are laid down on a 2048^3 mesh. We have used a new parallel particle-mesh (PM) + tree *N*-body code (Dubinski et al. 2004) to increase the spatial dynamic range. The gravitational force softening parameter is set to 0.1 times the mean particle separation. The particle mass is $1.6 \times 10^{12}\ h^{-1}\ M_{\odot}$, and the mean separation of particles is 2.75 h^{-1} Mpc, while that of SDSS galaxies in our best sample is about 6 h^{-1} Mpc. The simulation was started at $z = 17$ and followed the gravitational evolution of the CDM particles at 170 time steps using 128 CPUs on the IBM p690+ supercomputer of the Korea Institute of Science and Technology Information.

We make 100 mock surveys in the 5632 h^{-1} Mpc simulation for each of our samples and subsamples and for each smoothing scale in both real and redshift space. The total number of mock surveys is 3600. We use these mock surveys to estimate the uncertainties and systematic biases in the measured genus and its related statistics. We randomly locate "observers" in the 5632 h^{-1} Mpc simulation at $z = 0$ and make volume-limited surveys as defined in Table 1. The number of galaxies in each mock survey is constrained to be almost equal to that of each observational sample. We analyze the resulting mock samples in exactly the same way that the observational data are analyzed.

Any systematic bias due to the finite number of galaxies or smoothing effects should also appear in the results of analysis of mock samples. Variation of the genus among the mock samples provides an estimate of the random uncertainties of the observations. We compare the mean genus and genus-related statistics of over 100 mock samples in real space with those from the whole simulation cube. Differences between the mock samples and full cube indicate systematic biases for which we then correct the observed values. With the exception of the plotted genus curves, we correct all results in this fashion. Note that we use the mock surveys in real space to estimate the systematic biases because it is only in the real space where the true values of the topology parameters can be measured by using all the simulation data. Sets of 100 mock surveys made in redshift space are used to estimate the uncertainties in the observed genus and its related statistics. The cosmological parameters used in our simulation are only slightly different from those applied to observational data. Hence, assuming the *WMAP* cosmological parameters are approximately correct, systematic bias correction factors and uncertainty limits should be correctly estimated from mock surveys.

5. GENUS RESULTS

5.1. *Overview*

For each of the volume-limited samples of the SDSS listed in Table 1, we compute the genus at 501 volume-fraction threshold levels spaced by $\delta\nu_f = 0.01$. The shortest smoothing length applied is set to about $(2 \ln 2)^{-1/2} \approx 0.85$ times the average intergalaxy separation $\bar{d} = \bar{n}^{-1/3}$, which corresponds to a Gaussian smoothing kernel whose FWHM is $2\bar{d}$.

To estimate the uncertainties of these measurements, in each case we use the variance among 100 mock surveys drawn from the 5632 h^{-1} Mpc ΛCDM simulation in redshift space. These uncertainties include the effects of both Poisson fluctuations and sample variance. Figures 6 and 8 show the genus curves and uncertainties. The smooth curve in each plot is the mean over 100 mock samples. To see the dependence of our results on the observer's location, we have made additional mock surveys at locations where the local overdensity smoothed over a 8 h^{-1} Mpc top hat is between 0 and 1, the peculiar velocity is 600 ± 50 km s^{-1}, and the peculiar velocity shear is $|v - \bar{v}|/\bar{v} < 0.5$. Here $\bar{v}$ is the bulk velocity of the 8 h^{-1} Mpc sphere around the particle (cf. Gorski et al. 1989). The resulting genus statistics are of little difference with those from random locations.

We then measure the amplitude $G_{\rm obs}$ of the best-fit Gaussian genus curve, the shift $\Delta\nu$, and the cluster and void multiplicity parameters A_C and A_V for each curve. Using results from the mock surveys, we correct these parameters for systematic effects that result from the shape of the survey volume (see § 4). Figures 7 and 9 present these parameters and compare them with results from mock surveys of the ΛCDM simulation. Table 2 lists all the measured parameters, both corrected (in parentheses) and uncorrected for systematics. Note that the figures plot the genus per smoothing volume, $gR_{\rm G}^3 = (G_{\rm obs}/V_{\rm survey})R_{\rm G}^3$, rather than $G_{\rm obs}$. It can be seen in Table 2 that the systematic biases are smaller for cases with smoothing lengths shorter than the mean galaxy separation of a given sample.

In the following sections, we examine the dependence of the genus on both the smoothing scale and the luminosity of galaxies. Note that we test for luminosity bias using subsamples that cover the same physical volume (same angular and comoving distance limits), so that there are no sample variance effects.

5.2. *Scale Dependence*

To test for dependence of the genus parameters on smoothing scale, we begin by examining the best sample (see Table 1 and Fig. 3). Genus curves measured from the best sample at smoothing scales $R_{\rm G} = 5$, 6, and 8 h^{-1} Mpc are shown in Figure 6 (*top*). The genus-related statistics with the systematic biases corrected are shown in Figure 7 (*middle five points*) and summarized in Table 2 for five smoothing lengths, $R_{\rm G} = 5, 6, 7, 8$, and 9 h^{-1} Mpc.

The top panel of Figure 7 shows the genus density per smoothing volume $gR_{\rm G}^3$. The middle panel shows the shift parameter $\Delta\nu$. The bottom panel shows the cluster and void multiplicity parameters A_C (*filled symbols*) and A_V (*open symbols*), respectively. The shaded areas indicate the 1 σ limits calculated from 100 mock surveys from the ΛCDM simulation. In the bottom panel, shaded areas are not shown for A_V.

TABLE 2

GENUS-RELATED STATISTICS OF THE OBSERVATIONAL SAMPLES AND SUBSAMPLES

Sample Name	$\bar{d}$[a] (h^{-1} Mpc)	R_G[b] (h^{-1} Mpc)	G_{obs}	$\Delta\nu$	A_V	A_C
Scale Dependence						
Sparse.....	11.31	9.5	68.5(56.7) ± 5.6	−0.10(−0.02) ± 0.04	0.72(0.80) ± 0.07	1.29(1.30) ± 0.12
	...	11.0	41.0(36.0) ± 4.1	−0.06(−0.00) ± 0.05	0.74(0.80) ± 0.09	1.45(1.45) ± 0.17
Best	6.14	5.0	125.4(103.3) ± 9.7	−0.17(−0.05) ± 0.03	0.69(0.78) ± 0.05	0.80(0.86) ± 0.08
	...	6.0	77.3(69.7) ± 7.3	−0.15(−0.08) ± 0.05	0.71(0.75) ± 0.07	0.74(0.75) ± 0.08
	...	7.0	52.3(49.8) ± 5.6	−0.15(−0.10) ± 0.06	0.70(0.72) ± 0.09	0.74(0.73) ± 0.10
	...	8.0	36.2(35.2) ± 4.9	−0.15(−0.11) ± 0.07	0.74(0.75) ± 0.12	0.69(0.66) ± 0.11
	...	9.0	25.0(24.8) ± 4.0	−0.145(−0.12) ± 0.08	0.79(0.79) ± 0.16	0.74(0.71) ± 0.14
Dense.....	4.17	3.5	24.1(19.7) ± 4.1	0.18(0.32) ± 0.078	0.42(0.46) ± 0.08	1.21(1.34) ± 0.28
	...	4.0	15.6(13.6) ± 3.2	0.18(0.27) ± 0.094	0.54(0.57) ± 0.13	1.26(1.30) ± 0.34
	...	4.5	10.4(9.4) ± 2.4	0.19(0.26) ± 0.106	0.46(0.46) ± 0.14	1.14(1.17) ± 0.37
Luminosity Dependence						
L1	7.17	6.0	85.3(71.8) ± 7.5	−0.11(−0.01) ± 0.04	0.80(0.89) ± 0.08	0.98(1.03) ± 0.11
L1-1.....	9.04	7.5	47.2(39.3) ± 4.6	−0.14(−0.12) ± 0.05	0.76(0.85) ± 0.11	1.01(1.04) ± 0.13
L1-2.....	9.04	7.5	47.0(39.2) ± 4.6	−0.09(−0.06) ± 0.05	0.93(1.05) ± 0.13	0.91(0.94) ± 0.12
L1-3.....	9.04	7.5	44.5(37.1) ± 4.3	−0.09(−0.06) ± 0.05	0.91(1.02) ± 0.13	0.98(1.02) ± 0.13
L2	4.71	4.0	80.8(67.4) ± 8.6	−0.04(0.07) ± 0.05	0.81(0.89) ± 0.10	0.87(0.95) ± 0.11
L2-1.....	5.94	5.0	46.9(39.2) ± 6.1	−0.13(−0.03) ± 0.07	0.80(0.89) ± 0.12	0.65(0.68) ± 0.10
L2-2.....	5.94	5.0	47.9(40.0) ± 6.2	−0.05(0.05) ± 0.07	0.77(0.85) ± 0.12	0.72(0.75) ± 0.11
L2-3.....	5.94	5.0	46.4(38.8) ± 6.0	−0.06(0.05) ± 0.07	0.90(0.99) ± 0.14	0.82(0.85) ± 0.13
L3	4.44	3.8	39.1(33.3) ± 6.0	0.04(0.16) ± 0.07	0.62(0.67) ± 0.09	1.13(1.21) ± 0.20
L3-1.....	5.54	5.0	19.5(16.5) ± 3.7	0.02(0.11) ± 0.09	0.89(0.95) ± 0.20	1.11(1.14) ± 0.24
L3-2.....	5.54	5.0	22.0(18.6) ± 4.1	0.03(0.13) ± 0.09	0.65(0.69) ± 0.15	0.99(1.02) ± 0.22
L3-3.....	5.54	5.0	20.8(17.6) ± 3.9	0.08(0.18) ± 0.09	0.60(0.64) ± 0.14	1.03(1.06) ± 0.22
L4	4.09	3.5	23.3(19.4) ± 3.9	0.12(0.24) ± 0.09	0.44(0.48) ± 0.09	1.23(1.34) ± 0.31
L4-1.....	5.16	4.4	12.8(10.5) ± 2.5	0.02(0.13) ± 0.11	0.47(0.52) ± 0.12	1.15(1.24) ± 0.36
L4-2.....	5.16	4.4	11.7(9.6) ± 2.3	0.12(0.23) ± 0.11	0.44(0.49) ± 0.12	1.37(1.48) ± 0.43
L4-3.....	5.16	4.4	10.5(8.7) ± 2.1	0.09(0.21) ± 0.11	0.61(0.67) ± 0.16	1.38(1.50) ± 0.43

NOTES.—G_{obs} is the amplitude of the observed genus curve, $\Delta\nu$ is the shift parameter, and A_C and A_V are the cluster and void abundance parameters, respectively. Uncertainty limits are estimated from mock surveys in redshift space, and systematic bias corrected values are given in parentheses.

[a] Mean separation.

[b] Smoothing length.

In the top panel of Figure 7 we find that the genus per smoothing volume gR_G^3 slightly rises with smoothing scale. This trend is as expected. For a simple power-law spectrum of density fluctuations, the genus density per smoothing volume is proportional to $(n+3)^{1.5}$ (Melott et al. 1988), where n is the power index of the power spectrum, $P(k) \propto k^n$, of the galaxy distribution. However, because the CDM power spectrum has a maximum at a larger wavelength than any smoothing scale that we apply, we expect to measure higher genus density per smoothing volume as we increase R_G in the case of the ΛCDM model.

The middle panel of Figure 7 shows that the shift parameter for the best sample is negative, $\Delta\nu < 0$, and is well below the ΛCDM prediction. On a smoothing scale of 6 h^{-1} Mpc, the probability of observing a lower value of $\Delta\nu$ in the ΛCDM model is $P = 0.02$. Thus, the best sample exhibits a strong meatball (cluster dominated) shift.

The cluster multiplicity A_C for the best sample is consistently below unity (see Fig. 7, *bottom*) and below the ΛCDM prediction, indicating that there are fewer independent isolated high-density regions than for a Gaussian random field or the ΛCDM model. The probability of finding a lower value of A_C with a smoothing scale of 6 h^{-1} Mpc in the ΛCDM model is only $P = 0.03$.

The strong meatball shift ($\Delta\nu < 0$) and low cluster multiplicity ($A_C < 1$) in the best sample are probably caused by the Sloan Great Wall in region 1 and the X-shaped structure in region 2. The wall is located at a distance between about 160 and 240 h^{-1} Mpc and is almost fully contained in the best sample.

We find that the void multiplicity parameter, A_V, is much lower than 1 at all smoothing scales explored (see Fig. 7, *bottom*). This implies that voids are more connected than is expected for Gaussian fields. Park et al. (2005) find that nonlinear gravitational evolution causes the A_V parameter to rise but that A_V can become lower than unity when a proper prescription for biased galaxy formation is applied. Thus, the observation that $A_V < 1$ is strong evidence for biased galaxy formation. This measurement of small-scale topology provides a new quantitative test for galaxy formation theories. Here we find that the scale dependence of genus indicates that A_V only weakly depends on the smoothing scale. In contrast with the observed void multiplicity, the A_V parameter of the ΛCDM matter field (not shown in Fig. 7) is greater than 1 at scales smaller than about 9 h^{-1} Mpc (Park et al. 2005). Although the mock surveys are constructed by treating all matter particles as candidate galaxies, and their topology is not to be directly compared with that of observed galaxies, it still provides some guideline. Note that in the early topology analyses dark matter particles are often used for this comparison (Canavezes et al. 1998; Protogeros & Weinberg 1997). Simple prescriptions like the peak biasing scheme are also often used (Park & Gott 1991; Vogeley et al. 1994; Colley et al. 2000). When the purpose of topology analysis is to discriminate among different galaxy formation mechanisms using observational data,

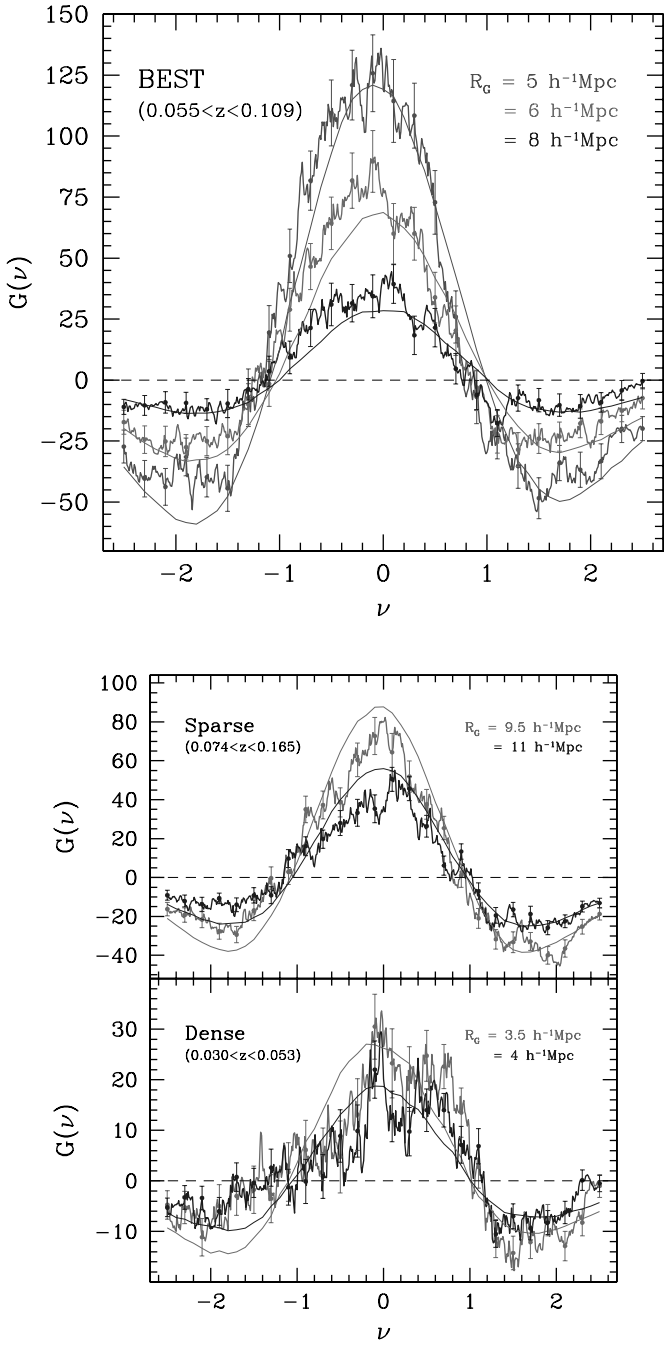

FIG. 6.—*Top*: Genus curves measured from the best sample at three smoothing scales. Solid curves are the genus curves averaged over 100 mock surveys in a ΛCDM simulation in redshift space at the same smoothing lengths. These curves have not been corrected for systematic uncertainties. *Bottom*: Similar genus curves for the sparse and dense samples and corresponding mock surveys. [*See the electronic edition of the Journal for a color version of this figure*.]

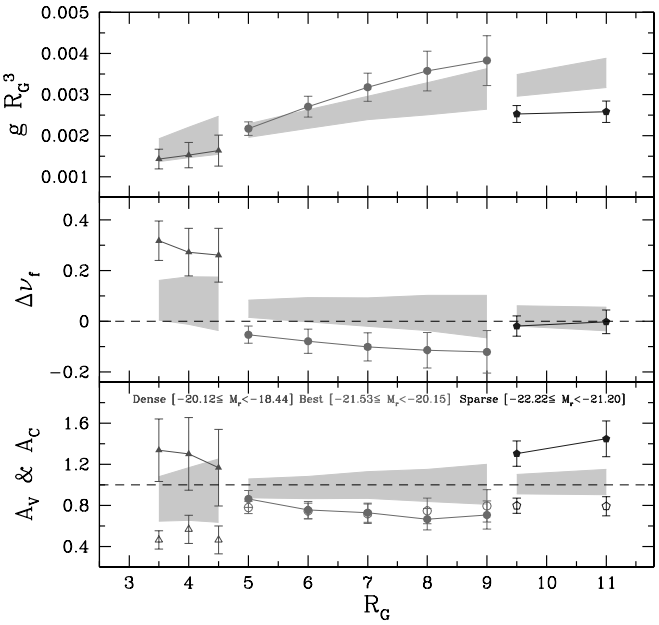

FIG. 7.—Genus-related statistics as a function of the Gaussian smoothing length R_G. Systematic bias corrections are made using mock surveys in real space of the ΛCDM model. Uncertainty limits are derived from mock surveys in redshift space. The shaded areas denote the 1 σ upper and lower limits estimated from the mock samples. In the bottom panel, A_C is given by filled symbols, A_V is given by open symbols, and the shaded areas are shown only for A_C. [*See the electronic edition of the Journal for a color version of this figure*.]

one should apply proper prescriptions for identifying galaxies in the *N*-body simulation.

For comparison to the best sample, we also examine the genus curves of the sparse and dense samples, as shown in Figure 6 (*bottom*) at two smoothing scales, plotted together with the mean genus curves from 100 mock surveys. The parameters gR_G^3, $\Delta\nu$, A_C, and A_V for the dense sample are the leftmost three points in each panel of Figure 7, while the rightmost two points in each panel show results for the sparse sample.

The genus amplitude of the sparse sample is significantly lower than that of the ΛCDM model. We do not think that this is a real signal but rather that this result has been caused by a lack of bright galaxies at far distances in sample 14. The number density of galaxies in volume-limited samples, defined by absolute magnitude limits, starts to radially decrease when the absolute magnitude limit exceeds −22. Paucity of bright galaxies can be easily noticed in Figure 3 at absolute magnitudes $M_r \leq -22.5$ and redshift $z \geq 0.13$ (see also Fig. 3 of Tegmark et al. [2004], who took into account the evolution of galaxies). The lower density of galaxies at the far side of the sparse sample effectively decreases the sample volume at a given threshold level and thus decreases the amplitude of the genus curve.

The dense sample shows a clear positive shift $\Delta\nu > 0$ when compared with the matter distribution of the ΛCDM model. This shift is caused mainly by the luminosity bias, which is described below in § 5.3.

In both the dense and sparse samples we find that the cluster multiplicity A_C is somewhat larger than that for the ΛCDM simulation. But the A_C of the sparse sample seems overestimated due to the radial density drop, which causes individual galaxies at the far side to appear as isolated high-density regions. The void multiplicity A_V for the dense and sparse samples is less than unity, in agreement with the results for the best sample. Therefore, we find a low value of A_V in all of these samples.

Within each of the samples (best, dense, and sparse), we find no clear evidence for scale dependence of the parameters $\Delta\nu$, A_C, or A_V. As discussed above, the increase of gR_G^3 with smoothing scale is as expected for a CDM-like power spectrum.

5.3. *Topology as a Function of Galaxy Luminosity*

It is well known that the strength of galaxy clustering depends on luminosity (Park et al. 1994; Norberg et al. 2001; Zehavi et al. 2005; Tegmark et al. 2004). Park et al. (1994) demonstrated that this luminosity bias is due to bright galaxies that tend to populate only dense regions and completely avoid voids. To study the

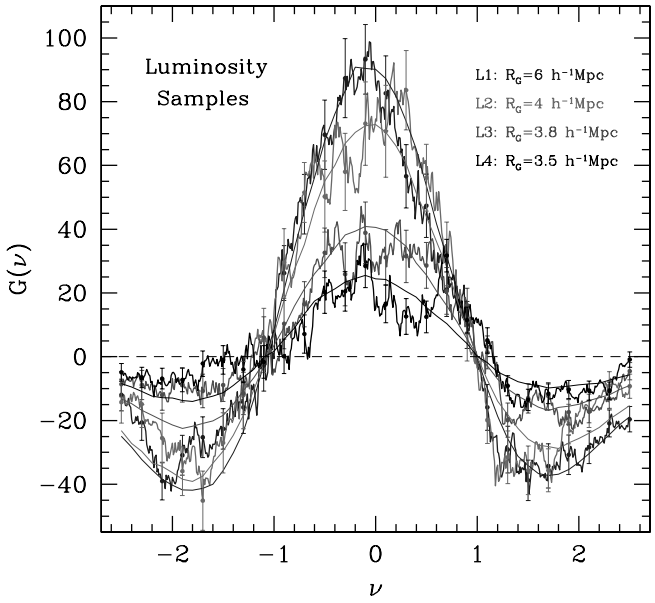

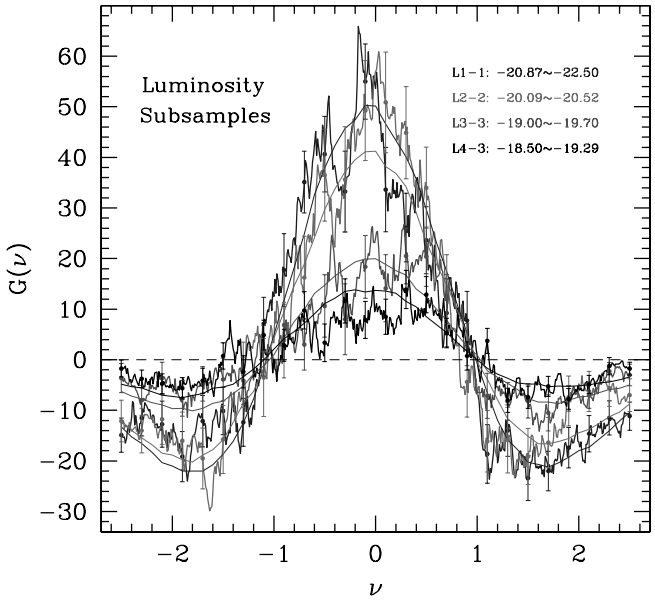

FIG. 8.—*Top*: Genus curve calculated using all galaxies contained in each luminosity sample. The smoothing length is roughly 0.85 times the mean separation between galaxies in each luminosity sample. *Bottom*: Genus curves of luminosity subsamples that have half the number of galaxies contained in their parent luminosity samples. Only one subsample for each luminosity sample is shown. Smoothing lengths are 7.5, 5.0, 5.0, and 4.4 h^{-1} Mpc for the L1-1, L2-2, L3-3, and L4-3 subsamples, respectively. [*See the electronic edition of the Journal for a color version of this figure*.]

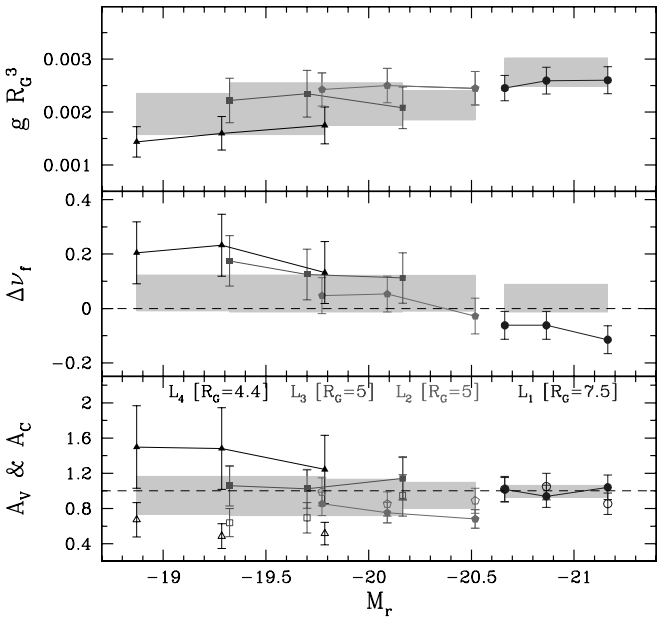

FIG. 9.—Genus-related statistics for luminosity subsamples (see Table 1 for definitions). The measured values of subsamples that belong to the same luminosity sample are connected together, except for the A_V parameter. The smoothing lengths adopted are $R_G = 7.5$, 5.0, 5.0, and 4.4 h^{-1} Mpc for the subsamples of L1, L2, L3, and L4, respectively. Shaded regions are the 1 σ variation regions calculated from 100 mock surveys. In the bottom panel, A_C is given by filled symbols, A_V is given by open symbols, and the shaded areas are shown only for A_C. [*See the electronic edition of the Journal for a color version of this figure*.]

galaxy luminosity bias beyond one-point and two-point statistics (e.g., Jing & Börner [2004] and Kayo et al. [2004] for the three-point correlation function, Hikage et al. [2003] for Minkowski functionals), here we test for luminosity bias in the topology of the large-scale structure of galaxies.

For this analysis we construct four luminosity samples, L1, L2, L3, and L4, each of which spans an absolute magnitude range $\Delta M_r = 2$ (see Fig. 3 and Table 1 for definitions). Figure 8 presents the genus curves calculated for these luminosity samples. Table 2 lists the measured genus-related statistics. The smoothing lengths are set to be about 0.85 times the mean separation between galaxies. The genus curves averaged over 100 mock luminosity samples are also plotted as smooth curves. We estimate uncertainties in the genus curves using the variance among the mock samples.

The genus curve for the brightest sample, L1, shows a clear negative shift $\Delta\nu < 0$ with respect to the mock survey result, while the faintest sample, L4, shows a clear positive shift $\Delta\nu > 0$. After systematic biases are corrected, using the mock surveys in real space, we find that the negative shift for sample L1 is reduced (see values in parentheses in Table 2) and that the fainter samples show even stronger positive shifts. The large significance of the change from negative (or zero) shift in bright samples to a positive genus shift in fainter samples seems to indicate luminosity bias effects on topology. However, we must be cautious because these samples cover different physical volumes; it might be the case that this trend is produced by local variation in topology.

To remove this ambiguity, we divide each luminosity sample into three subsamples that cover the same volume of space but with different absolute magnitude limits and with exactly half the number of galaxies as in the parent sample (see Table 1 for definitions). For example, the brighter upper half of galaxies in luminosity sample L1 is called L1-1 and the fainter half L1-3. The middle subsample, L1-2, overlaps with the brighter and fainter ones in absolute magnitude. Again, we set the smoothing lengths to about 0.85 times the galaxy mean separation. The measured statistics are listed in Table 2 and plotted in Figure 9. In Figure 9 each subsample appears as one point at the median absolute magnitude of galaxies in the subsample.

The differences among the subsamples drawn from a luminosity sample must be purely due to the luminosity bias, apart from variations caused by Poisson fluctuations. The luminosity bias of topology is most clearly detected in the case of the shift parameter. In all luminosity samples, the faintest subsample has a positive shift relative to the brightest one (see Fig. 9, *middle*).

The trend across the parent luminosity samples is also consistent with this phenomenon. This trend is particularly obvious in the case of samples L2 and L3, for which the smoothing length is the same. The transition from positive to negative shift appears to occur at around the characteristic absolute magnitude for SDSS galaxies, $M_{r*} = -20.44$.

Only the L2 and L3 samples are analyzed at the same smoothing scales; thus, their genus amplitudes can be directly compared. We find no statistically significant trend in the genus density among subsamples within each luminosity sample or across the luminosity samples. However, a weak dependence on luminosity can be seen, in the sense that brighter galaxies have higher genus density.

We find no systematic trend for the cluster and void multiplicity parameters, A_C and A_V, except that the A_V parameter is somewhat lower for the faintest luminosity sample, L4.

To see the luminosity bias more clearly, in Figure 8 (*bottom*) we plot the genus curves of luminosity subsamples whose absolute magnitude intervals do not overlap with one another. The systematic change in the shift of the genus curves toward positive ν is evident as the luminosity of the subsamples decreases (see Fig. 9). These curves are plotted alongside genus curves averaged over 100 mock surveys that simulate the luminosity subsamples. Note that the A_C parameter is exceptionally low in the case of subsamples of the L2 sample, where the Sloan Great Wall is fully contained.

Our finding that the genus curves for galaxies fainter than M_* tend to have positive shifts implies that the density field of this class of galaxies has a bubble-shifted topology ($\Delta\nu > 0$). In other words, the distribution of faint galaxies, which is less clustered than that of bright galaxies (as measured by the amplitude of the two-point correlation function), has empty regions nearly devoid of faint (as well as bright) galaxies. Furthermore, we find that underdense regions are more connected to one another than is expected for a Gaussian field ($A_V < 1$), and this shift is particularly evident in the distribution of faint galaxies. In contrast, bright galaxies show a meatball shift ($\Delta\nu \lesssim 0$): they form isolated clusters and filaments surrounded by large, empty spaces.

6. CONCLUSIONS

The SDSS is now complete enough to allow us to study the three-dimensional topology of the galaxy distribution and its dependence on physical properties of galaxies. We analyze the large-scale structure data set sample 14 of the New York University Value-Added Galaxy Catalog derived from the SDSS. In particular, we study the dependence of the topology of the large-scale structure on the smoothing scale and the galaxy luminosity. Although the angular mask of sample 14 is still very complicated, we are able to measure the genus statistic accurately by making extensive and careful use of mock surveys generated from a new large-volume *N*-body simulation.

Overall, the observed genus curves strongly resemble the random phase genus curve (see Fig. 6). This supports the idea that the observed structure arises from random quantum fluctuations, as predicted by inflation. But on top of this general pattern we observe small deviations, as might arise from nonlinear gravitational evolution (Melott et al. 1988; Park & Gott 1991; Matsubara 1994) and biasing (Gott et al. 1996).

We find a statistically significant scale dependence in the amplitude of the genus curve in the case of the best sample (Fig. 7 *top*). This scale dependence, which is expected in a ΛCDM universe, is consistent with the results of mock surveys in a ΛCDM model over the smoothing scales explored.

The A_V parameter, a measure of void multiplicity, is found to be smaller than 1 at all smoothing scales explored, from 3.5 to 11 h^{-1} Mpc. Since this parameter cannot become less than 1 through gravitational evolution, it provides strong evidence for biased galaxy formation in low-density environments. Galaxies form in such a way that underdense regions can be more connected than expected in the unbiased galaxy formation process of initially Gaussian fluctuations. The observed connectivity of voids could also arise for some special class of initial conditions, such as the bubbly density field in the extended inflationary scenario (La & Steinhardt 1989). This measurement using genus statistics provides a new constraint on models for galaxy biasing.

In our scale dependence study, we note that the shift parameter, $\Delta\nu$, is more negative and that the cluster multiplicity parameter, A_C, is smaller than those predicted by ΛCDM for mock surveys of the best sample. We attribute these phenomena to large, connected, high-density regions, such as the Sloan Great Wall and an X-shaped structure that runs several hundred megaparsecs across the survey volume. The statistical significance level is about 3 σ. More realistic mock galaxy catalogs that include biasing and more completed SDSS data are needed to draw conclusions on the consistency between the ΛCDM model and the observed universe. We have also found a paucity of galaxies brighter than about $M_r = -22$ at large distances in sample 14. Volume-limited samples constrained by absolute magnitude cuts brighter than -22 in sample 14 have radial density gradients and are thus not suitable for measuring parameters like the genus amplitude.

We clearly detect the signature of luminosity bias of the topology through the shift parameter $\Delta\nu$. We find that the genus of bright galaxies is more negatively (i.e., meatball) shifted than that of faint ones. The transition from negative to positive shift occurs at close to the characteristic magnitude $M_{r*} = -20.44$ of SDSS galaxies. This difference in the topology of bright and faint galaxies provides a further test for galaxy biasing models.

We test for a scale dependence of this luminosity bias by comparing the genus-related parameters of the brighter subset (L2-1) of luminosity sample L2 with those of the fainter subset (L2-3) at smoothing lengths 5, 6, and 7 h^{-1} Mpc. Given the uncertainties in the measured statistics, we do not find such a scale dependence.

To visually demonstrate variations in the spatial distribution of galaxies with different luminosity, in Figure 10 we plot the comoving distances and survey longitudes of galaxies in sample L2. Crosses and open circles are galaxies brighter than about M_*, while filled circles indicate galaxies fainter than about M_*. It is evident that faint galaxies are found in both low- and high-density environments, while brighter galaxies (e.g., Fig. 10, *crosses*) are rarely found in low-density regions. Because galaxies fainter than M_* fill the universe more uniformly but are still absent within large tunnels and voids, their distribution has more of a bubble topology. Galaxies brighter than M_* delineate dense clusters, filaments, and walls, surrounded by large, empty spaces, which fill most volume of the universe. Accordingly, they show a shift toward a meatball topology. The galaxy biasing mechanism should not only make brighter galaxies harder to form in underdense environments and cluster more strongly, but it should also make the distributions of bright and faint galaxies have meatball- and bubble-shifted topologies, respectively. It is not clear whether or not simple galaxy formation prescriptions like the semianalytic and numerical models (Berlind et al. 2003; Kravtsov et al. 2004; Zheng et al. 2005) or halo occupation distribution modeling of

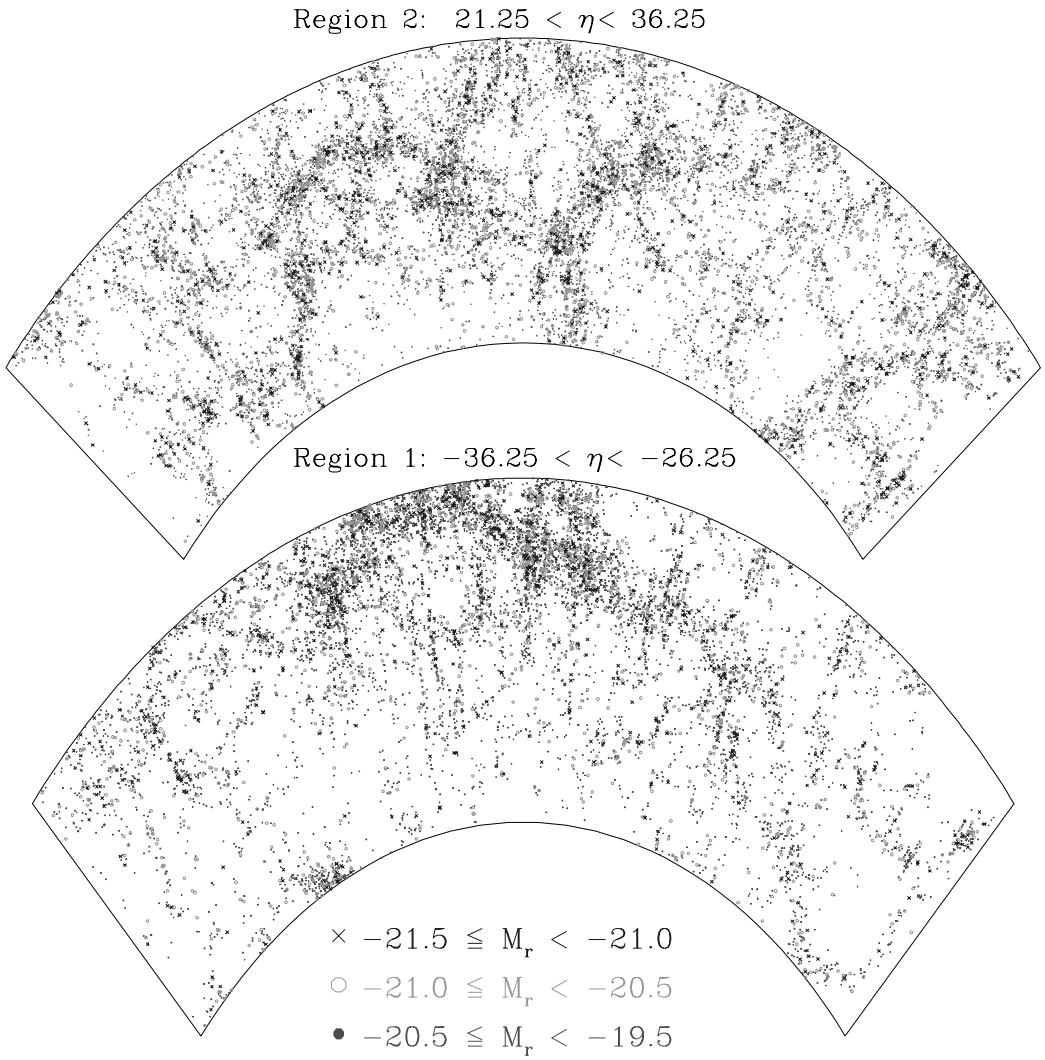

FIG. 10.—Distribution of galaxies in luminosity sample L2 in the comoving distance vs. survey longitude coordinate plane projected to the median volume latitude. Galaxies are distinguished by color and point type in accordance with their absolute magnitudes. Crosses are the brightest, open circles are of intermediate brightness, and filled circles are the faintest. [*See the electronic edition of the Journal for a color version of this figure*.]

galaxy formation (Ma & Fry 2000; Berlind & Weinberg 2002) satisfy these constraints. We plan to study this in future work.

C. B. P. acknowledges the support of the Korea Science and Engineering Foundation (KOSEF) through the Astrophysical Research Center for the Structure and Evolution of the Cosmos (ARCSEC) and through grant R01-2004-000-10520-0. M. S. V. acknowledges support from NASA grant NAG-12243. J. R. G. has been supported by NSF grant AST 04-06713.

Funding for the creation and distribution of the SDSS Archive has been provided by the Alfred P. Sloan Foundation, the participating institutions, the National Aeronautics and Space Administration, the National Science Foundation, the US Department of Energy, the Japanese Monbukagakusho, and the Max Planck Society. The SDSS Web site is http://www.sdss.org/.

The SDSS is managed by the Astrophysical Research Consortium (ARC) for the participating institutions. The participating institutions are the University of Chicago, Fermilab, the Institute for Advanced Study, the Japan Participation Group, the Johns Hopkins University, the Korean Scientist Group, Los Alamos National Laboratory, the Max-Planck-Institute for Astronomy (MPIA), the Max-Planck-Institute for Astrophysics (MPA), New Mexico State University, University of Pittsburgh, University of Portsmouth, Princeton University, the United States Naval Observatory, and the University of Washington.

REFERENCES

Abazajian, K., et al. 2003, AJ, 126, 2081
———. 2004, AJ, 128, 502
Adler, R. J. 1981, The Geometry of Random Fields (Chichester: Wiley)
Berlind, A. A., & Weinberg, D. H. 2002, ApJ, 575, 587
Berlind, A. A., et al. 2003, ApJ, 593, 1
Blanton, M. R., Lin, H., Lupton, R. H., Maley, F. M., Young, N., Zehavi, I., & Loveday, J. 2003a, AJ, 125, 2276
Blanton, M. R., et al. 2003b, AJ, 125, 2348
———. 2005, AJ, 129, 2562
Canavezes, A., et al. 1998, MNRAS, 297, 777
Colley, W. N., Gott, J. R., Weinberg, D. H., Park, C., & Berlind, A. A. 2000, ApJ, 529, 795
Doroshkevich, A. G. 1970, Astrophysics, 6, 320
Dubinski, J., Kim, J., Park, C., & Humble, R. 2004, NewA, 9, 111
Eisenstein, D. J., et al. 2001, AJ, 122, 2267
Fukugita, M., Ichikawa, T., Gunn, J. E., Doi, M., Shimasaku, K., & Schneider, D. P. 1996, AJ, 111, 1748
Geller, M. J., & Huchra, J. P. 1989, Science, 246, 897

Gorski, K. M., Davis, M., Strauss, M. A., White, S. D. M., & Yahil, A. 1989, ApJ, 344, 1
Gott, J. R., Cen, R., & Ostriker, J. P. 1996, ApJ, 465, 499
Gott, J. R., Jurić, M., Schlegel, D., Hoyle, F., Vogeley, M. S., Tegmark, M., Bahcall, N., & Brinkmann, J. 2005, ApJ, 624, 463
Gott, J. R., Melott, A. L., & Dickinson, M. 1986, ApJ, 306, 341
Gunn, J. E., et al. 1998, AJ, 116, 3040
Hamilton, A. J. S., Gott, J. R., & Weinberg, D. 1986, ApJ, 309, 1
Hamilton, A. J. S., & Tegmark, M. 2004, MNRAS, 349, 115
Hikage, C., et al. 2002, PASJ, 54, 707
———. 2003, PASJ, 55, 911
Hogg, D. W., Baldry, I. K., Blanton, M. R., & Eisenstein, D. J. 2002, preprint (astro-ph/0210394)
Hogg, D. W., Finkbeiner, D. P., Schlegel, D. J., & Gunn, J. E. 2001, AJ, 122, 2129
Hoyle, F., et al. 2002, ApJ, 580, 663
Jing, Y. P., & Börner, G. 2004, ApJ, 607, 140
Kayo, I., et al. 2004, PASJ, 56, 415
Kravtsov, A. V., Berlind, A. A., Wechsler, R. H., Klypin, A. A., Gottlober, S., Allgood, B., & Primack, J. R. 2004, ApJ, 609, 35
La, D., & Steinhardt, P. J. 1989, Phys. Rev. Lett., 62, 376
Lupton, R. H., Gunn, J. E., Ivezić, Ž., Knapp, G. R., Kent, S., & Yasuda, N. 2001, in ASP Conf. Ser. 238, Astronomical Data Analysis Software and Systems X, ed. F. R. Harnden, Jr., F. A. Primini, & H. E. Payne (San Francisco: ASP), 269
Ma, C., & Fry, J. N. 2000, ApJ, 543, 503
Matsubara, T. 1994, ApJ, 434, L43
Melott, A. L., Weinberg, D. H., & Gott, J. R. 1988, ApJ, 328, 50
Norberg, P., et al. 2001, MNRAS, 328, 64
Park, C., & Gott, J. R. 1991, ApJ, 378, 457
Park, C., Gott, J. R., & Choi, Y. 2001, ApJ, 553, 33
Park, C., Gott, J. R., Melott, A. L., & Karachentsev, I. D. 1992, ApJ, 387, 1
Park, C., Kim, J., & Gott, J. R. 2005, ApJ, 633, 1
Park, C., Vogeley, M. S., Geller, J., & Huchra, J. P. 1994, ApJ, 431, 569
Pier, J. R., Munn, J. A., Hindsley, R. B., Hennessy, G. S., Kent, S. M., Lupton, R. H., & Ivezić, Ž. 2003, AJ, 125, 1559
Protogeros, Z. A. M., & Weinberg, D. H. 1997, ApJ, 489, 457
Richards, G. T., et al. 2002, AJ, 123, 2945
Schlegel, D. J., Finkbeiner, D. P., & Davis, M. 1998, ApJ, 500, 525
Smith, J. A., et al. 2002, AJ, 123, 2121
Spergel, D. N., et al. 2003, ApJS, 148, 175
Stoughton, C., et al. 2002, AJ, 123, 485
Strauss, M. A., et al. 2002, AJ, 124, 1810
Tegmark, M., et al. 2004, ApJ, 606, 702
Vogeley, M. S., Park, C., Geller, M. J., Huchra, J. P., & Gott, J. R. 1994, ApJ, 420, 525
Weinberg, D. H. 1988, PASP, 100, 1373
Weinberg, D. H., Gott, J. R., & Melott, A. L. 1987, ApJ, 321, 2
York, D., et al. 2000, AJ, 120, 1579
Zehavi, I., et al. 2005, ApJ, 630, 1
Zheng, Z., et al. 2005, ApJ, in press (astro-ph/0408564)